

Effective work function of metals interfaced with dielectrics: A first-principles study of the Pt-HfO₂ interface

H. Zhu and R. Ramprasad*

*Chemical, Materials and Biomolecular Engineering and Institute of Materials Science,
University of Connecticut, 97 North Eagleville Road, Storrs, Connecticut 06269, USA*

(Received 12 January 2011; published 25 February 2011)

A parameter-free methodology to determine the *effective* work function, defined as the work function of the metal on the dielectric side of a metal-dielectric interface, is presented. This method relies on the direct determination of the effective work function through the interfacial dipole moment from standard density functional theory calculations devoid of scaling the band gap and band offset. For the case of a Pt-HfO₂ interface, this strategy is combined with statistical thermodynamic principles to predict the most probable effective work function at given combinations of temperature and O₂ pressure (through determination of the most favored interfacial O coverage). The predicted results are in excellent agreement with observations.

DOI: [10.1103/PhysRevB.83.081416](https://doi.org/10.1103/PhysRevB.83.081416)

PACS number(s): 73.30.+y, 71.15.Mb

It is well known that the vacuum work function of a metal surface is modulated by species present at the surface due to a modified surface dipole layer.¹⁻³ A similar phenomenon occurs when a metal is interfaced with an insulator. Here, the vacuum levels on either side of the interface may be misaligned [cf. Fig. 1(b)]. The degree of such a misalignment will depend on the magnitude of the interfacial dipole moment, which is determined by the interfacial atomic and electronic structures.^{4,5} The vacuum level discontinuity across the interface implies that the work function of the metal on the vacuum side (ϕ) may, in general, be different from that on the insulator side. The latter is generally referred to as the *effective* work function (ϕ_{eff}),^{6,7} and is of paramount importance in situations that involve metal electrodes. In this contribution, we present a simple parameter-free methodology to directly and unambiguously determine ϕ_{eff} for a metal-insulator system. Furthermore, by combining this method with first-principles thermodynamics, we provide a general prescription to understand the correlation between ϕ_{eff} and processing conditions that control the metal-insulator interfacial structure and dipole.

A notable example where the above considerations are particularly relevant is the emerging “high- k ” microelectronic device, which involves an interface between a metal and a high dielectric constant (i.e., “high- k ”) material such as HfO₂.⁸⁻¹⁰ In such devices, the metal work function is required to be 4.1 or 5.2 eV, so that the metal Fermi level (E_F) is aligned, respectively, to the conduction band minimum (CBM) or the valence band maximum (VBM) of the underlying Si substrate.¹¹ However, as noted above, even if a metal with the appropriate vacuum work function value is used, the work function of the metal on the oxide side of the interface shifts with respect to its vacuum value.¹² Moreover, the degree of this shift depends on the processing conditions that the device is subjected to.^{7,13-16} Figure 1 shows a schematic of the band and potential lineups for a metal slab and a metal-oxide interface. Several theories exist to explain the process-induced variations of ϕ_{eff} .^{7,17-21} These include Fermi-level-pinning at the metal-dielectric interface and the presence of O vacancies in the HfO₂ layer or at the metal-dielectric interface.

In past work based on density functional theory (DFT) computations, ϕ_{eff} of metals interfaced with oxides have generally been estimated using the following equation:²²⁻²⁴

$$\phi_{\text{eff}} = \chi + E_g - \text{VBO}, \quad (1)$$

where χ , E_g , and VBO are the electron affinity, the band gap of dielectric, and the valence band offset (in this case, the Schottky barrier height) between the metal and dielectric (see Fig. 1). Standard DFT calculations, due to approximations to the electronic exchange-correlation potential and energy, can not correctly predict any of these three terms, especially χ and E_g .²⁵ The conventional procedure to handle this issue has been to use experimental values for χ and E_g and/or scale VBO by the ratio of the experimental to the computed values of E_g .²⁴

In this paper, we formally relate ϕ_{eff} to the metal-oxide interface dipole moment and present a simple fully *ab initio* procedure (devoid of scaling or fitting) to determine ϕ_{eff} from standard DFT calculations. For definiteness, we choose Pt as the metal and HfO₂ as the dielectric in this paper, as this is one of the best-characterized metal and high- k interfaces. For this system, ϕ_{eff} is observed to be less than the vacuum value of 5.8 eV, and varies significantly (4.6–5.5 eV) with processing conditions.^{7,13-16} Such changes in ϕ_{eff} have been attributed to varying levels of O at the Pt-HfO₂ interface.⁷ Using well-established first-principles thermodynamics principles,²⁶ we have determined the most probable O concentration at the Pt-HfO₂ interface for a given combination of temperature (T) and O₂ pressure (P_{O_2}) (Ref. 27), the process variables, and have determined ϕ_{eff} corresponding to these interfacial O coverages. The predicted ϕ_{eff} values of Pt-HfO₂ are in excellent agreement with experimental observations.

Our DFT calculations were performed using the VASP code²⁸ with the PW91 generalized gradient approximation²⁹ (GGA) and the projector-augmented wave approach.³⁰ The calculated lattice parameters for bulk m -HfO₂ are 5.09 Å for a , 5.14 Å for b , and 5.27 Å for c , in good agreement with the corresponding experimental values (5.12, 5.17, and 5.29 Å, respectively).³¹ The predicted lattice parameter for fcc-Pt is 3.98 Å, compared to the experimental value of 3.92 Å.³²

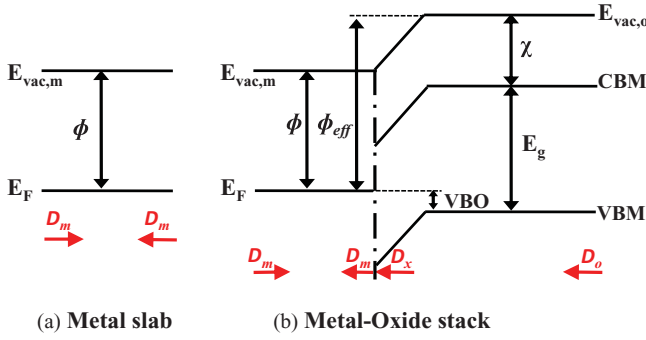


FIG. 1. (Color online) Schematic of (a) the macroscopic band structure of a metal slab and (b) the band alignment in a metal-oxide stack. $E_{vac,m}$ and E_F are, respectively, the vacuum level and Fermi level of the metal. $E_{vac,o}$, CBM, VBM, χ , and E_g are, respectively, the vacuum level, conduction band minimum, valence band maximum, electron affinity, and band gap of the oxide. VBO stands for valence band offset, and represents the energy difference between the metal Fermi level and the oxide VBM. D_m and D_o are the surface dipole moments of the metal free surface and the oxide free surface, respectively. D_x is excess interfacial dipole moment, i.e., the total interfacial dipole moment minus the metal free surface dipole moment.

Following prior work,³³ the interface models were created by placing a strained (111) ($2 \times \sqrt{3}$) Pt slab on top of a (001) (1×1) m -HfO₂ slab [Fig. 2(a)] along with a vacuum region of 10 Å, which required a $5 \times 5 \times 1$ Monkhorst-Pack k -point mesh to yield converged results. Dipole corrections were used to handle the asymmetric nature of the heterostructures considered.

First-principles thermodynamic theories were applied first to identify stable Pt-HfO₂ interfaces. Various interfacial O coverages, represented as θ_O in units of a monolayer (ML), at the Pt-HfO₂ interface were considered, ranging from 0 to 2 in steps of 0.25 ML. In keeping with the stoichiometry of HfO₂, an ML is defined as two times the number of Hf atoms in a layer. The corresponding interface configurations are denoted by Pt: θ_O :HfO₂. Three representative interface

structures are shown in Fig. 2(a). When $\theta_O = 0$ ML, the interface is represented by Pt-Hf bonding. For $\theta_O = 1$, one half of the O atoms passivates the interfacial Hf atoms and the other half bonds to interfacial Pt atoms. The local structure of Pt-O bonding at the Pt:2:HfO₂ interface (i.e., $\theta_O = 2$) mimics a structure akin to distorted platinum oxide. These three interfaces are referred to as “clean,” “abrupt,” and “oxidized,” respectively.

The interface energy of each structure relative to the interface energy for $\theta_O = 0.5$ is defined as

$$\gamma_{\theta_O} = [E_{Pt:\theta_O:HfO_2} - E_{Pt:0.5:HfO_2} - (2\theta_O - 1)\mu_{O_2}(T, P_{O_2})]/A, \quad (2)$$

where $E_{Pt:\theta_O:HfO_2}$ is the DFT (or 0 K) energy for the interface model. We note that only relative interface energies are important in this study, and have arbitrarily chosen the Pt:0.5:HfO₂ interface to be the reference (the Hf and O atoms are in the 1:2 ratio for this heterostructure slab). $\mu_{O_2}(T, P_{O_2})$ is the chemical potential of one O₂ molecule, which can be obtained from thermochemical tables,³⁴ or determined *ab initio* based on statistical thermodynamics.²⁷ Although vibrational and configurational contributions of the interface to the relative interface energy are neglected here, we have shown elsewhere that they do not make significant changes to the interface phase diagrams.²⁷ By identifying the lowest interface energy structure for each (T, P_{O_2}) condition, we have obtained the interface phase diagram for the Pt-HfO₂ interface, which is shown in Fig. 2(b). Under typical processing conditions [the shaded region in Fig. 2(b)], the stable interface O coverage between Pt and HfO₂ varies between 0.5 and 1 ML over a wide temperature range. With the decrease of T or increase of P_{O_2} , the stable interface O coverage will increase from 0 ML (clean interface) smoothly to ~ 1 ML (abrupt interface) and then abruptly to 2 ML (oxidized interface). This oxidation behavior is similar to the surface oxidation of the (111) Pt surface.³⁵ Further details concerning the determination of the interface phase diagram are documented separately elsewhere.²⁷

Next, we discuss the methodology to determine ϕ_{eff} using the interface dipole moment for the structures identified above and the Pt vacuum work function (both of which are well represented in standard DFT calculations). As schematically shown in Fig. 1, when the metal slab with a surface dipole moment of D_m and a vacuum work function of ϕ is interfaced with an oxide, an extra dipole moment (D_x) is created at the interface, and hence results in a vacuum level discontinuity across the interface. ϕ and the vacuum level discontinuity (through D_x) determine ϕ_{eff} as

$$\phi_{eff} = \phi + 4\pi D_x/A, \quad (3)$$

where A is the interface area. The calculated ϕ for the strained (111) Pt surface [required to form a coherent interface with (1×1) (001) HfO₂ as described previously] is 5.75 eV and the corresponding value for the Pt slab at equilibrium is 5.7 eV (consistent with the experimental value of 5.8 eV).¹⁶ In other words, ϕ is found to be somewhat insensitive to the strain in the metal slab. As shown in Fig. 1(b), the asymmetric interface supercell used in the current calculations contains two free surfaces: the metal and the oxide free surfaces with surface dipole moments of D_m and D_o , respectively. Thus

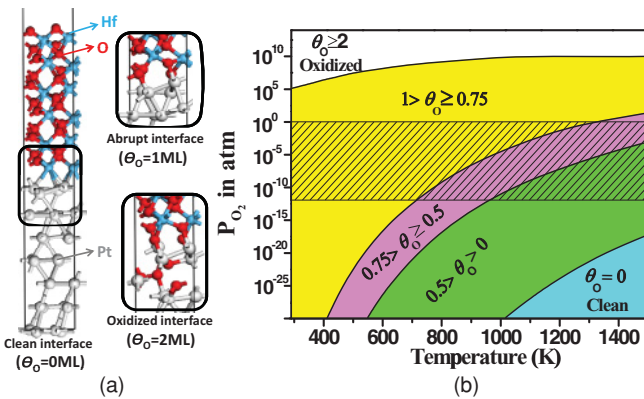


FIG. 2. (Color online) (a) Atomic structures of Pt: θ_O :HfO₂ interfaces with $\theta_O = 0, 1$, and 2 ML; (b) The interface phase diagram for Pt: θ_O :HfO₂. The boundaries between two different stable interface structures are represented by the black curves. The shaded region represents the regime of expected processing conditions.

TABLE I. The effective work function (ϕ_{eff}) along with the additional oxide-induced interfacial dipole moment per unit interface area (D_x/A) for Pt: θ_{O} :HfO₂ interfaces. The calculated vacuum work function of strained Pt is 5.75 eV. The ϕ_{eff} values corresponding to the interface structure present in the interface phase diagram [Fig. 2(b)] are shown in **bold** so as to distinguish these from the values for unstable structures (not seen in the interface phase diagram). The sign of (D_x/A) indicates that it is directed into the metal surface.

θ_{O} (ML)	D_x/A (eV)	ϕ_{eff} (eV)
0	-0.162	3.71
0.25	-0.136	4.04
0.5	-0.111	4.35
0.75	-0.024	5.45
1	-0.013	5.59
1.25	-0.003	5.71
1.5	0.021	6.02
1.75	-0.003	5.71
2	-0.031	5.36

[cf. Fig. 1(b)], the net dipole moment of the supercell D_n (which may be unambiguously computed as done by VASP), is $D_x + D_o$, from which D_x may be determined using

$$D_x = D_n - D_o. \quad (4)$$

We note that D_o may be computed from a separate (001) m -HfO₂ slab calculation with the same surface termination as the oxide free surface in the interface model, i.e., half ML O layer [cf. Fig. 2(a)]. The obtained dipole moment per unit surface area (D_o/A) is 0.072 eV.

Based on Eq. (3) and DFT determinations for ϕ and D_x , we have obtained ϕ_{eff} for the different Pt: θ_{O} :HfO₂ cases considered; these are listed in Table I. The ϕ_{eff} values corresponding to the stable interface structure present in the interface phase diagram [Fig. 2(b)] are shown in **bold** so as to distinguish these from the values for unstable structures (not seen in the interface phase diagram). As we can see from Table I, D_x , and hence ϕ_{eff} , are strongly dependent on the interfacial O content. ϕ_{eff} of the stable interfaces increases from

3.71 to 5.45 eV as θ_{O} increases from 0 to 0.75 ML. Further oxidation of Pt:0.75:HfO₂ to Pt:2:HfO₂ only decreases ϕ_{eff} by ~ 0.09 eV, indicating that the saturation ϕ_{eff} for Pt-HfO₂ is ~ 5.45 eV. We also note that all computed ϕ_{eff} values for stable interfaces are smaller than the vacuum work function of Pt.

Next, we discuss the T and P_{O_2} dependence of ϕ_{eff} . In the sense that a statistical distribution of ϕ_{eff} values is expected for each (T, P_{O_2}) condition, the Pt-HfO₂ stack will display an average ϕ_{eff} value ($\bar{\phi}_{\text{eff}}$). $\bar{\phi}_{\text{eff}}$ may be defined as

$$\begin{aligned} \bar{\phi}_{\text{eff}} &= \sum_{\theta_{\text{O}}=0}^2 \phi_{\text{eff}}(\theta_{\text{O}}) \times \wp(\theta_{\text{O}}) \\ &= \sum_{\theta_{\text{O}}=0}^2 \phi_{\text{eff}}(\theta_{\text{O}}) \times \frac{\exp(-\gamma_{\theta_{\text{O}}}/kT)}{\sum_{\theta_{\text{O}}=0}^2 \exp(-\gamma_{\theta_{\text{O}}}/kT)}, \end{aligned} \quad (5)$$

where $\phi_{\text{eff}}(\theta_{\text{O}})$ and $\wp(\theta_{\text{O}})$ are the ϕ_{eff} value and the probability of a coverage of θ_{O} . The determined $\bar{\phi}_{\text{eff}}$ as a function of T and P_{O_2} for Pt-HfO₂ is portrayed in Fig. 3. As we can see, $\bar{\phi}_{\text{eff}}$ decreases with T and increases with P_{O_2} . This finding is consistent with prior experimental work in which a Pt-HfO₂ stack annealed in forming gas and O₂ gas displayed an effective work function of 4.6 and 4.9 eV, respectively.⁷ Furthermore, the shaded region in Fig. 3 represents the expected, or generally adopted, processing conditions (from the standard pressure to the ultrahigh vacuum conditions). The predicted $\bar{\phi}_{\text{eff}}$ at these expected annealing conditions (4.4–5.5 eV) is in favorable agreement with the reported experimental values (4.6–5.5 eV).^{7,13–15} More quantitative comparisons between our work and experiments is not possible at this time, as available experimental studies do not provide the exact processing O₂ pressure.

Finally, we note that several simplifying assumptions have been made to make our calculations tractable. These include constraints imposed by periodicity and coherency, and consideration of only a single-crystal environment. Nevertheless, we believe the dominant factors that control the thermodynamics and the electronic structure of the interface are largely *local*, which are indeed well captured by our treatment. Our prior work on the thermodynamics of Pt-HfO₂ as well as Si-HfO₂ interfaces provide partial justification for these hopes and beliefs.²⁷ In that work, it was shown that the conditions at which certain interface phases are favored are indeed predicted with remarkable accuracy, despite the simplifying assumptions made. It was also shown that strains induced by the requirement of coherency in our treatment alter our conclusions negligibly.

In summary, a parameter-free methodology to directly determine the effective work function of a metal-dielectric interface in terms of the interfacial dipole moment has been presented. The variation of the effective work function with respect to the environment (in this case, T and P_{O_2}), attributed to changes in the interfacial O content, has been captured using first-principles thermodynamics. The favorable agreement between the computed and experimental results for the Pt-HfO₂ interface under generally adopted processing conditions is indicative of the usefulness of such full first-principles property-processing relationship studies. Such approaches

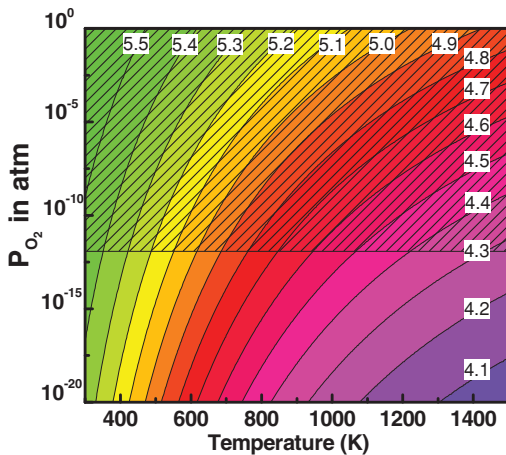


FIG. 3. (Color online) $\bar{\phi}_{\text{eff}}$ as a function of temperature (T) and O₂ pressure (P_{O_2}). The shaded region represents the regime of expected processing conditions.

may be effectively used in *ab initio* materials design attempts to tailor the interfacial dipole moment.

The authors would like to acknowledge the financial support of this work by the National Science Foundation (NSF), com-

putational support through allocations at the NSF Teragrid, and a critical reading of the manuscript by Leonardo Fonseca. R. R. would also like to acknowledge helpful discussions with Matthias Scheffler and support from the Alexander von Humboldt Foundation.

*Current address: The Fritz-Haber-Institut der MPG, Berlin, Germany; rampi@ims.uconn.edu

¹A. Kiejna, K. F. Wojciechowski, *Metal Surface Electron Physics* (Elsevier, Oxford, 1996).

²P. C. Rusu and G. Brocks, *J. Phys. Chem. B* **110**, 22628 (2006).

³R. Ramprasad, P. von Allmen, and L. R. C. Fonseca, *Phys. Rev. B* **60**, 6023 (1999).

⁴M. Peressi, N. Binggeli, and A. Baldereschi, *J. Phys. D: Appl. Phys.* **31**, 1273 (1998).

⁵J. D. Burton and E. Y. Tsybmal, *Phys. Rev. B* **82**, 161407 (2010).

⁶J. L. Freeouf and J. M. Woodall, *Appl. Phys. Lett.* **39**, 727 (1981).

⁷J. K. Schaeffer, L. R. C. Fonseca, S. B. Samavedam, Y. Liang, P. J. Tobin, and B. E. White, *Appl. Phys. Lett.* **85**, 1826 (2004).

⁸R. M. Wallace and G. D. Wilk, *Crit. Rev. Solid State Mater. Sci.* **28**, 231 (2003).

⁹B. H. Lee, J. Oh, H. H. Tseng, R. Jammy, and H. Huff, *Mater. Today* **9**, 32 (2006).

¹⁰B. H. Lee, S. C. Song, and P. Kirsch, *IEEE Trans. Electron Devices* **55**, 8 (2008).

¹¹J. Westlinder, G. Sjöblom, and J. Ollsson, *Microelectron. Eng.* **75**, 389 (2004).

¹²Y. C. Yeo, T. J. King, and C. H. Hu, *J. Appl. Phys.* **92**, 7266 (2002).

¹³C.-H. Lu, G. M. T. Wong, M. D. Deal, W. Tsai, P. Majhi, C. O. Chui, M. R. Visokay, J. J. Chambers, L. Colombo, B. M. Clemens, and Y. Nishi, *IEEE Electron Device Lett.* **26**, 445 (2005).

¹⁴D. Gu, S. K. Dey, and P. Majhi, *Appl. Phys. Lett.* **89**, 082907 (2006).

¹⁵H. Yang, Y. Son, S. Baek, and H. Hwang, *Appl. Phys. Lett.* **86**, 092107 (2005).

¹⁶M. T. Paffett, S. C. Gebhard, R. G. Windham, and B. E. Koel, *J. Phys. Chem.* **94**, 6831 (1990).

¹⁷J. Robertson, *J. Vac. Sci. Technol. B* **18**, 1785 (2000).

¹⁸Y. Kita, S. Yoshida, T. Hosoi, T. Shimura, K. Shiraishi, Y. Nara, K. Yamada, and H. Watanabe, *Appl. Phys. Lett.* **94**, 122905 (2009).

¹⁹X. P. Wang *et al.*, *IEEE Electron Device Lett.* **28**, 258 (2007).

²⁰H.-C. Wen *et al.*, *Microelectron. Eng.* **85**, 2 (2008).

²¹O. Sharia, K. Tse, J. Robertson, and A. A. Demkov, *Phys. Rev. B* **79**, 125305 (2009).

²²K. Xiong, P. Delugas, J. C. Hooker, V. Fiorentini, J. Robertson, D. Liu, and G. Pourtois, *Appl. Phys. Lett.* **92**, 113504 (2008).

²³E. Cho, B. Lee, C.-K. Lee, S. Han, S. H. Jeon, B. H. Park, and Y.-S. Kim, *Appl. Phys. Lett.* **92**, 233118 (2008).

²⁴L. R. C. Fonseca and A. A. Knizhnik, *Phys. Rev. B* **74**, 195304 (2006).

²⁵A. Alkauskas, P. Broqvist, F. Devynck, and A. Pasquarello, *Phys. Rev. Lett.* **101**, 106802 (2008).

²⁶K. Reuter and M. Scheffler, *Phys. Rev. Lett.* **90**, 046103 (2003).

²⁷H. Zhu, C. Tang, and R. Ramprasad, *Phys. Rev. B* **82**, 235413 (2010).

²⁸G. Kresse and J. Furthmüller, *Phys. Rev. B* **54**, 11169 (1996).

²⁹J. P. Perdew, J. A. Chevary, S. H. Vosko, K. A. Jackson, M. R. Pederson, D. J. Singh, and C. Fiolhais, *Phys. Rev. B* **46**, 6671 (1992).

³⁰P. E. Blochl, *Phys. Rev. B* **50**, 17953 (1994); G. Kresse and D. Joubert, *ibid.* **59**, 1758 (1999).

³¹J. Adam and M. D. Rodgers, *Acta Crystallogr.* **12**, 951 (1959).

³²Ralph W. G. Wyckoff, *The Structure of Crystals* (Reinhold, New York, 1935), p. 11.

³³A. V. Gavrikov, A. A. Knizhnik, A. A. Bagatur'yants, B. V. Potapkin, L. R. C. Fonseca, M. W. Stoker, and J. Schaeffer, *J. Appl. Phys.* **101**, 014310 (2007).

³⁴D. R. Stull and H. Prophet, *JANAF Thermodynamical Tables*, 2nd ed. (US National Bureau of Standards, Washington, DC, 1971).

³⁵U. Engstrom and R. Ryberg, *Phys. Rev. Lett.* **82**, 2741 (1999).